Elucidation of the Electrochemical Reaction Mechanism in MFe2O4 (M=Ni, Co) Conversion-Type Negative Electrode Systems by using In Situ X-ray Absorption Spectroscopy

ARTICLE · JULY 2015

READS
62

9 AUTHORS, INCLUDING:

Geethu Balachandran
Karlsruhe Institute of Technology
3 PUBLICATIONS **0** CITATIONS
SEE PROFILE

Ditty Dixon
Karlsruhe Institute of Technology
16 PUBLICATIONS **107** CITATIONS
SEE PROFILE

Aiswarya Bhaskar
Karlsruhe Institute of Technology
11 PUBLICATIONS **65** CITATIONS
SEE PROFILE

Stefan Mangold
Karlsruhe Institute of Technology
45 PUBLICATIONS **300** CITATIONS
SEE PROFILE

ChemPubSoc Europe

DOI: 10.1002/celc.201500197

CHEMELECTROCHEM Articles

Special Issue

Elucidation of the Electrochemical Reaction Mechanism in MFe_2O_4 (M = Ni, Co) Conversion-Type Negative Electrode Systems by using In Situ X-ray Absorption Spectroscopy

Geethu Balachandran,[a] Ditty Dixon,*[a] Natalia Bramnik,[a] Aiswarya Bhaskar,[a] Murat Yavuz,[a, b] Lukas Pfaffmann,[a] Frieder Scheiba,[a] Stefan Mangold,[c] and Helmut Ehrenberg[a]

Mixed transition-metal ferrites with the chemical formula MFe_2O_4 (M = Co, Ni), synthesized through an inverse co-precipitation route, were characterized by using scanning electron microscopy and powder X-ray diffraction, which demonstrate phase-pure compounds with particle sizes of about 100 nm. Cyclic voltammetry investigations in lithium half-cells revealed a difference between the first cycle and the following charge–discharge cycles, which is characteristic for conversion-type electrode systems. To understand the mechanism of the electrochemical reaction in the first cycle, in situ X-ray absorption spectroscopy was performed during cycling at a charge–discharge rate of C/10. During the first discharge process, the crystalline Co and Ni ferrites undergo reduction. A coexistence of binary metal oxides (CoO/NiO and Fe_2O_3) and metallic phases were observed during the discharge. At the end of discharge, only the existence of metallic nanoclusters was observed. In the subsequent charging process, Fe was found to undergo complete oxidation in both ferrites. In contrast, almost 60% of the Co or Ni remained in the metallic state at the end of the charge (end of first cycle). This incomplete oxidation of Co and Ni in the applied voltage range could be the main reason behind the irreversible capacity loss and low coulombic efficiency often reported for these conversion electrode systems.

1. Introduction

The demand for better Li-ion batteries for various applications necessitates the development of new electrode materials with improved energy density, cycle life, safety and low cost. Owing to their numerous properties, nanostructured materials are widely used for enhancing the power density in rechargeable lithium-ion batteries.[1] In particular, electrode systems that operate through a reversible electrochemical conversion mechanism have been receiving a lot of interest, owing to their intrinsically higher capacity compared to intercalation-type electrodes.[2]

For 3D metal oxides operating through a conversion mechanism, the initial discharge results in the transformation of the initial compound into a composite material consisting of metallic nanoparticles (2–8 nm) dispersed in a Li_2O matrix at the end of discharge. The internal formation of nanostructured materials during the first reduction cycle leads to a higher packing density and, therefore, a higher volumetric energy density in comparison with most nanomaterials used as negative electrode systems. Moreover, the redox potential of conversion-type electrode systems can be tuned through the electronegativity of the anion. Among the anodes that operate through a conversion mechanism, binary transition-metal oxide,[2–8] nitrides,[9,10] sulfides,[11–13] and phosphides[14] are already being investigated.

Fe-containing oxides are particularly interesting as conversion-type materials, as iron is cost effective and environmentally friendly. The presence of Fe nanograins in the Li_2O matrix after electrochemical lithiation of Fe_2O_3 has been confirmed by using in situ transmission electron microscopy.[15] The reaction was found to be only partially reversible; the delithiated product was not Fe_2O_3, but FeO. Recently, a combined powder X-ray diffraction (XRD) and X-ray absorption spectroscopy (XAS) study was performed to characterize the structural evolution of spinel Fe_3O_4 upon lithiation.[16] The transformation of the spinel into the rock-salt structure was observed between 1.7 and 4 moles of Li insertion. At the end of the discharge, elemental Fe was not detectable by using XRD, probably because

[a] G. Balachandran, Dr. D. Dixon, Dr. N. Bramnik, Dr. A. Bhaskar, M. Yavuz, L. Pfaffmann, Dr. F. Scheiba, Dr. H. Ehrenberg
Institute for Applied Materials - Energy Storage Systems (IAM-ESS)
Karlsruhe Institute of Technology (KIT)
Hermann-von-Helmholtz-Platz 1
76344 Eggenstein-Leopoldshafen (Germany)
E-mail: ditty.dixon@kit.edu

[b] M. Yavuz
Helmholtz Institute Ulm (HIU)
Electrochemical Energy Storage
P. O. Box 3640,76021, Karlsruhe (Germany)

[c] Dr. S. Mangold
ANKA Synchrotron Radiation Facility
Karlsruhe Institute of Technology (KIT)
Hermann-von-Helmholtz-Platz 1
76344 Eggenstein-Leopoldshafen (Germany)

Special Issue An invited contribution to a Special Issue on In Situ Monitoring of Fuel Cell and Battery Processes

the cluster size was too small, but it was unambiguously evidenced by using extended X-ray absorption fine structure (EXAFS) analysis.

Transition-metal ferrites MFe_2O_4 (M = 3D transition metals) with the spinel structure have been extensively studied as anode materials; however, structural investigations of ternary iron-oxide systems upon conversion are scarce.[17–19] Such ternary metal oxides may provide improved electrochemical performance in comparison with binary ones. The partial substitution of Fe in the spinel structure with other 3D metals may influence the cation distribution in the spinel structure as well as the Li^+ solubility in these spinel ferrites during lithiation and delithiation. This may have further impact on phase transformations and the electrode microstructure during the conversion reaction.

In the present work, a comparative study of different metal ferrites MFe_2O_4 (M = Co, Ni), as anode materials for Li-ion batteries, is presented with respect to their electrochemical conversion mechanism. Owing to the availability of an appropriate ^{57}Co source and the favorable Debye temperatures, Mössbauer spectroscopy has been extensively used to investigate changes in the oxidation states and magnetic ordering of these ferrites materials when used as negative electrodes in Li-ion batteries.[19–21] However, these studies are often performed ex situ with different states of charge. Moreover, Mössbauer spectroscopy can only access chemical information around the Fe nuclei. Here, In situ XAS is applied to get an insight into the mechanism of the initial reduction of these materials in the electrochemical cell. Moreover, XAS studies can give element-specific information about the various atoms present in the material. Element-specific information is highly significant in the present study, as the material undergoes a complete phase transformation and individual metal oxides coexist at the end of the first charge–discharge cycle. Furthermore, materials that are investigated by using XAS do not require long-range order; therefore, even local nanostructures can be investigated as they are formed during conversion.

2. Results and Discussion

2.1. Electrochemical Characterization

The cyclic voltammetry (CV) results obtained for both anode materials ($CoFe_2O_4$ and $NiFe_2O_4$) between 0.1 and 3.1 V at a scan rate of 0.1 $mV s^{-1}$ for 30 cycles are shown in Figure 1.

The characteristic feature of the CV curves is the significant difference between the first and subsequent cycles, which is well known for conversion-type cathodes. A sharp cathodic peak was observed in the first cycle at around 0.57 V for $CoFe_2O_4$ and at 0.58 V for $NiFe_2O_4$, corresponding to the reduction of transition-metal ions to the metallic state and formation of Li_2O. The expected electrochemical reactions during the first discharge and subsequent charge are given below in Equations (1) and (2), respectively:

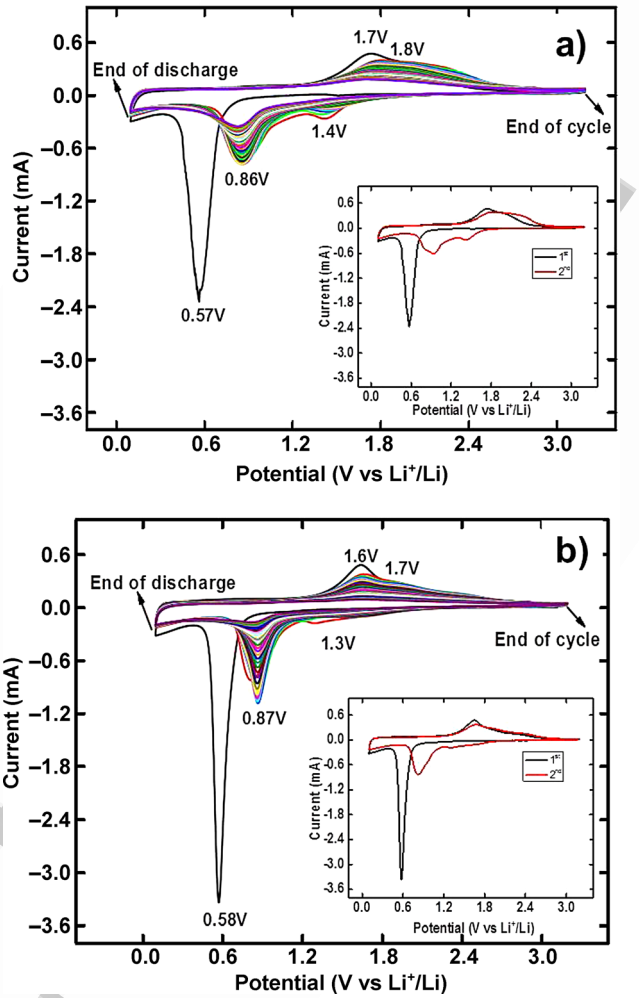

Figure 1. Cyclic voltammograms of a) $CoFe_2O_4$ and b) $NiFe_2O_4$.

$$CoFe_2O_4/NiFe_2O_4 + 8\,Li^+ + 8\,e^- \rightarrow 4\,Co/Ni + 2\,Fe + 4\,Li_2O \quad (1)$$

$$Co/Ni + 2\,Fe + 4\,Li_2O \rightarrow CoO/NiO + Fe_2O_3 + 8\,Li^+ + 8\,e^- \quad (2)$$

The increase in cathodic current at the end of discharge may indicate the reduction of the electrolyte, promoted by the presence of metal nanoparticles. The anodic part in the first cycle consists of two peaks, which are not very well resolved. These peaks are usually attributed to the oxidation of metal nanoparticles; nevertheless, at the end of this process, the spinel structure of the initial compound may not be restored. Upon second discharge, two cathodic peaks were observed at 0.86 and 1.4 V for $CoFe_2O_4$ and at 0.83 and 1.3 V for $NiFe_2O_4$, respectively.

2.2. Morphological and Structural Analyses

The synthesized 3D transition-metal ferrites annealed at 800 °C were characterized by using scanning electron microscopy (SEM) to reveal the morphology and particle size. The obtained results are displayed in Figure 2. The average particle size was

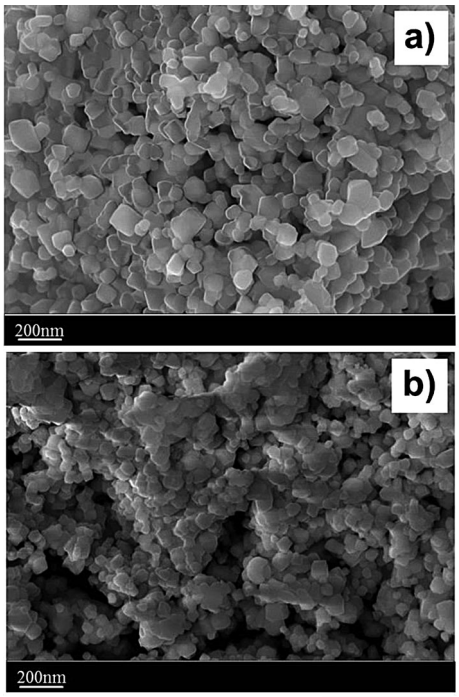

Figure 2. SEM images of a) $CoFe_2O_4$ and b) $NiFe_2O_4$.

estimated to be 69.9 ± 21.00 nm for $CoFe_2O_4$ and 52.3 ± 18.57 nm for $NiFe_2O_4$.

The XRD patterns obtained for the pristine $CoFe_2O_4$ and $NiFe_2O_4$ samples are displayed in Figure 3. Both the materials crystallize in an inverse cubic spinel structure and the patterns are indexed with the space group $Fd\bar{3}m$ (see Figure 3a and Figure 3b). The unit-cell parameters obtained from Rietveld refinement based on the obtained XRD data were 8.3725(2) and 8.3423(4) Å for $CoFe_2O_4$ and $NiFe_2O_4$ samples, respectively.

2.3. Oxidation-State Elucidation: In Situ and Ex Situ XAS

In situ XAS measurements were carried out during the first discharge and ex situ XAS was performed at the end of the complete cycle at a charge-discharge rate of C/10 in a voltage window 0.1–3 V. Figure 4 shows Li content (x) versus voltage (E_{we}) curve for $CoFe_2O_4$ and $NiFe_2O_4$ cycled against Li. Owing to the bulky construction of the in situ cell, the extracted Li amount is lower in case of the in situ experiments.

To obtain direct information about the oxidation states of Fe and Co/Ni in $CoFe_2O_4$ and $NiFe_2O_4$, the X-ray absorption near-edge structure (XANES) region of the XAS spectra of the samples at Fe and Co/Ni K edges were compared with the XANES region obtained from XAS spectra of different reference materials. XANES regions extend from approximately −20 eV below the absorbing edge to 100 eV above the edge of the XAS spectrum, and are often used in qualitative analyses. Therefore, the edge position and line shape obtained from the reference materials could be compared with any unknown sample, and information about the oxidation state and, to a certain extent, the coordination environment of the absorbing atom could be interpreted.

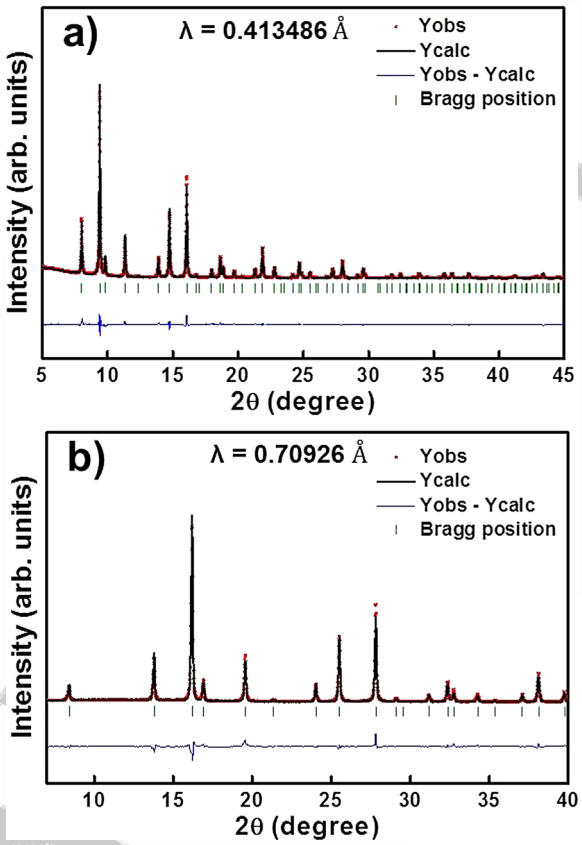

Figure 3. Rietveld refinement results based on XRD data for a) $CoFe_2O_4$ and b) $NiFe_2O_4$.

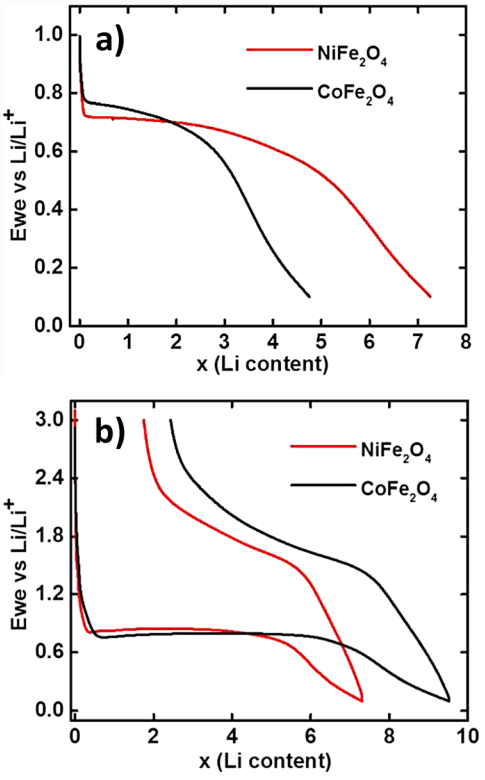

Figure 4. The x (Li content) versus voltage curve for $CoFe_2O_4$ and $NiFe_2O_4$ for a) in situ and b) ex situ XAS measurements.

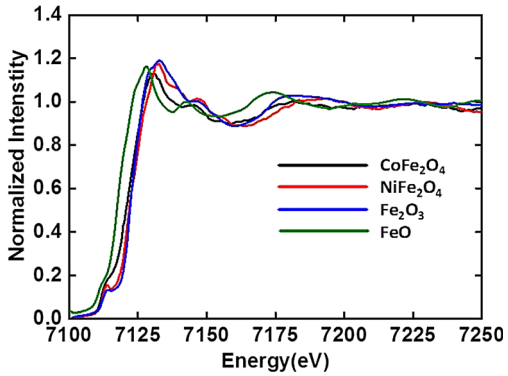

Figure 5. The Fe edge XANES region for both $CoFe_2O_4$ and $NiFe_2O_4$.

By comparing the XANES region obtained from the XAS spectra measured at the Fe K edge (Figure 5), it can be seen that the edge position of both samples overlaps with the edge position of the Fe_2O_3 sample, which is measured as the reference. Thus, it may be concluded that, in both ferrite samples, Fe has a formal valance state of Fe^{3+}, as in the case of Fe_2O_3. Moreover, it can also be seen that the Fe K edge, XANES region, line shape of both $CoFe_2O_4$ and $NiFe_2O_4$ are identical. Therefore, the local coordination of Fe in both the samples is almost identical. Similarly, by comparing the XANES region at Co and Ni edges with that of the XANES region (Figure 6a and Figure 6b) of the corresponding reference materials (CoO and NiO), a formal oxidation state of +2 can be assigned to both elements.

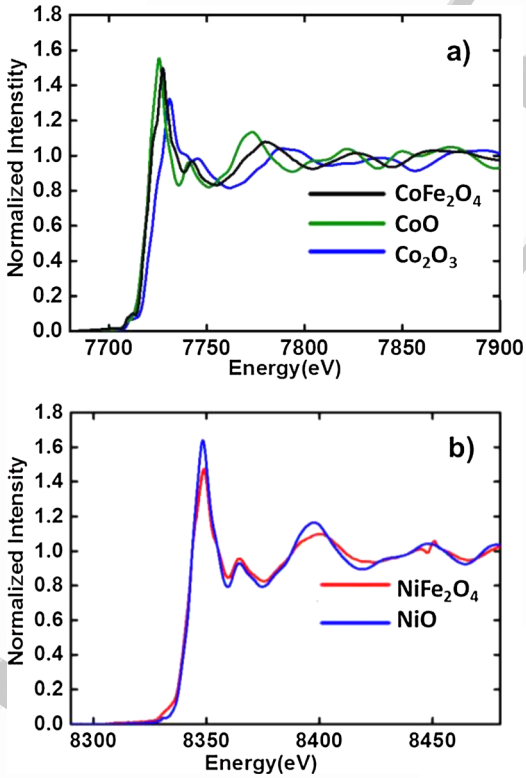

Figure 6. The Ni and Co edge XANES regions for both $CoFe_2O_4$ and $NiFe_2O_4$.

In contrast to the XANES region, the EXAFS region, which extends beyond 100 eV above the edge, can easily be modeled, owing to minor contributions from multiple scattering phenomena. The EXAFS information gives the local coordination environment around the adsorbing atom. First-shell EXAFS analysis at each edge within the available data range gives three nearest-neighbor bond distances. By combining the Fe K edge and Co K edge fits for the $CoFe_2O_4$ sample, two different oxygen bond distances can be seen for the sample, that is, a shorter Fe–O bond distance and a longer Co–O bond distance. The EXAFS fitting results are in agreement if an inverse spinel structure is assumed for $CoFe_2O_4$. In this structure, the Co atoms only occupy the octahedral sites and the Fe atoms occupy the tetrahedral and remaining octahedral sites. However, oxygen bond distances between Fe atoms occupying tetrahedral and octahedral sites cannot be resolved, owing the limitations in the available k space. In contrast, metal–metal shell fitting yielded, more or less, three bond distances with the possible combinations of Fe_{tera}–Fe_{tetra}, Fe_{tetra}–Co_{octa}, and Fe/Co_{octa}–Fe/Co_{octa}, which are the expected distances for inverse spinel coordination.[21] Similar fitting results were also obtained for Fe and Ni edge EXAFS analysis; therefore, an inverse spinel structure can also be assigned to $NiFe_2O_4$. The complete EXAFS analysis results are summarized in Table 1.

Table 1. EXAFS fit results obtained for Fe and Co/Ni K edges for $CoFe_2O_4$ and $NiFe_2O_4$.

Edge	Sample	Interatomic distance (r) [Å]	*DW* factor [Å^2]
Fe	$CoFe_2O_4$	(Fe–O) 1.98(1)	(Fe–O) 0.014(2)
		(Fe–Fe) 3.00(9)	(Fe–Fe) 0.009(2)
		(Fe–Co) 3.50(1)	(Fe–Co) 0.007(1)
Co	$CoFe_2O_4$	(Co–O) 2.03(1)	(Co–O) 0.012(2)
		(Co–Fe) 2.96(1)	(Co–Fe) 0.008(1)
		(Co–Co) 3.49(1)	(Co–Co) 0.006(1)
Fe	$NiFe_2O_4$	(Fe–O) 1.97(1)	(Fe–O) 0.015(2)
		(Fe–Fe) 2.99(1)	(Fe–Fe) 0.011 (1)
		(Fe–Ni) 3.47(1)	(Fe–Ni) 0.008 (1)
Ni	$NiFe_2O_4$	(Ni–O) 2.03(2)	(Ni–O) 0.008(3)
		(Ni–Fe) 2.92(2)	(Ni–Fe) 0.006(3)
		(Ni–Ni) 3.47(3)	(Ni–Ni) 0.009(4)

The in situ measurements for both $CoFe_2O_4$ and $NiFe_2O_4$ at Fe, Co, and Ni edges revealed edge shifts and changes in the XANES line shapes, which may be assigned to an oxidation state change as well as coordination changes around the absorbing atoms (Figure 7).

During the conversion reaction, it is expected that the ferrite materials can transform into their respective oxides and to metallic states. Coexistence of different phases can complicate the EXAFS analysis; therefore, to obtain information about the different phase fractions, linear combination fitting (LCF) analysis was applied to the XANES region at selected potentials. Reference materials, such as Fe_3O_4, Fe_2O_3, FeO, and Fe metal foil, were used for LCF analysis at the Fe K edge. For the LCF fitting at Co and Ni edges, CoO, Co metal, NiO, and Ni metal spectra were used as references. From the LCF analyses of both

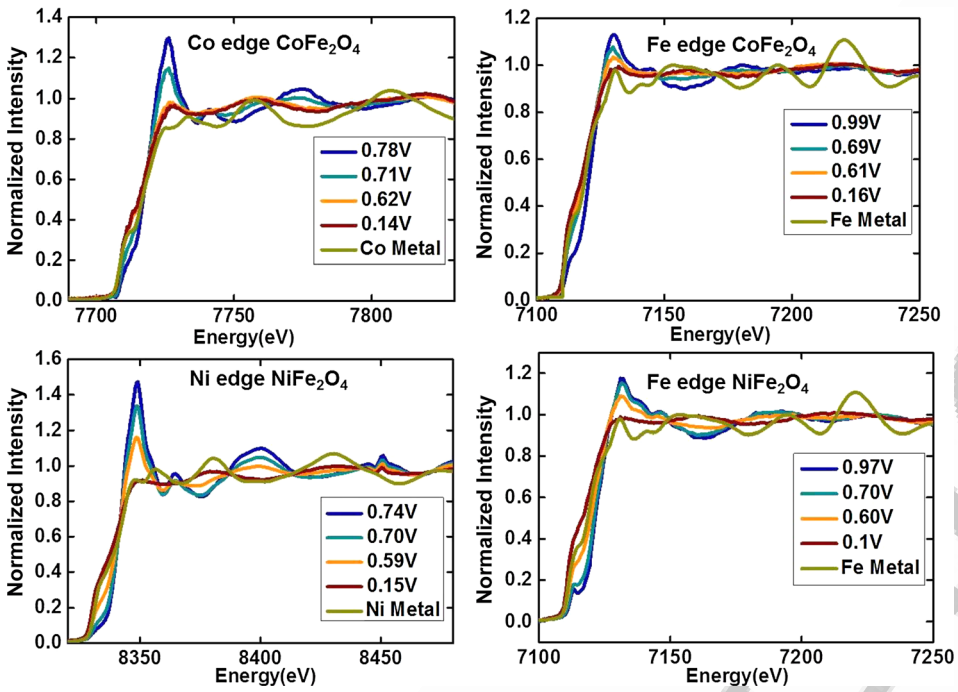

Figure 7. In situ XANES region obtained for $CoFe_2O_4$ and $NiFe_2O_4$.

$CoFe_2O_4$ and $NiFe_2O_4$ at Fe K edges, an increase in the Fe-metal fraction was observed with electrochemical reduction. Moreover, a small fraction of the FeO component could be fitted during the LCF analysis, indicating the formation of Fe^{2+} during reduction. At the end of the discharge, only a contribution from metallic Fe was observed at the Fe K edge. Similarly, at Co and Ni edges, a coexistence of the metal oxide and the metallic phase was observed during the discharge process. A complete transformation to metallic Co and Ni was detected at the end of discharge for $CoFe_2O_4$ and $NiFe_2O_4$, respectively. The LCF fitting results are summarized in Table 2.

The formation of metallic clusters for all of the transition elements can also be qualitatively inferred from the real space ("R space"). Fourier transform (FT) reveals one single peak around 2.3 Å, which corresponds to the respective metallic species. Note that, at all of the edges, the relative FT amplitude decreased during electrochemical reduction (Figure 8).

This effect can be attributed to the formation of metallic nano-domains during the conversion reaction. To verify this, EXAFS data at all edges were analyzed at the end of discharge, based on the structure model of a pure metal. EXAFS analyses of the pure fcc-metal foils yielded coordination numbers of 12. However, for the in situ measurements at the end of discharge, the coordination numbers for all metal–metal shells were considerably lower, confirming the formation of nano-metallic domains or clusters. However, the exact size of the formed nanoparticles cannot be deduced from the EXAFS analyses, as summarized in Table 3 for the end of discharge (between 0.1 and 0.2 V against Li^+/Li).

Finally, electrodes obtained at the end of the first cycle were subjected to ex situ XAS to obtain more information about the reversibility of the metallic phases formed at the end of first discharge to metal oxides. For both the $CoFe_2O_4$ and $NiFe_2O_4$ samples, it can be seen that the XANES line shape at the Fe edge of the pristine samples and the samples after the first cycle were almost identical (Figure 9).

However, the FT (inset) shows that the second shell, where the metal–metal interaction appears, has almost vanished for the samples after one complete cycle compared to the pristine samples. This conclusively proves that Fe metal formed during the first discharge has been completely retransformed into an amorphous or cluster-sized oxide phase. By comparing the edge position with the Fe reference material, a formal valance of +3 can be assigned to the Fe oxide that is formed. In contrast, for both Co and Ni edges, strong differences in the XANES line shapes were observed for pristine samples and those obtained after the first cycle. For both edges, the XANES region of the samples after one complete cycle, measured at the inflection point, is closer to that of a Co- or Ni-metal foil than for CoO or NiO (Figure 10).

Similarly, the FT (inset) at both Co and Ni edges for samples after one complete cycle show dominant peaks around 2.3 Å, which can be attributed to the presence of metallic domains. Therefore, it may be concluded that both metallic Co and Ni

Table 2. LCF fitting results at a) Fe K edge for $CoFe_2O_4$ and $NiFe_2O_4$ and b) Co/Ni K edge for $CoFe_2O_4$ and $NiFe_2O_4$ at different potentials. Contribution of each reference material at different potentials are tabulated.

a) Sample	Potential [V]	Contribution from Fe_2O_3	Contribution from FeO	Contribution from Fe
$CoFe_2O_4$	0.69	0.30	0.20	0.50
	0.61	0.20	0.15	0.65
	0.16	0.06	0.10	0.84
$NiFe_2O_4$	0.70	0.77		0.23
	0.60	0.44	0.06	0.50
	0.44	0.12	0.16	0.72
	0.1		0.15	0.85

b) Sample	Potential [V]	Contribution from CoO/NiO	Contribution from Co/Ni
$CoFe_2O_4$	0.71	0.6	0.4
	0.6	0.16	0.84
	0.16	0.06	0.94
$NiFe_2O_4$	0.70	0.72	0.28
	0.59	0.38	0.62
	0.44	0.06	0.94
	0.1		1

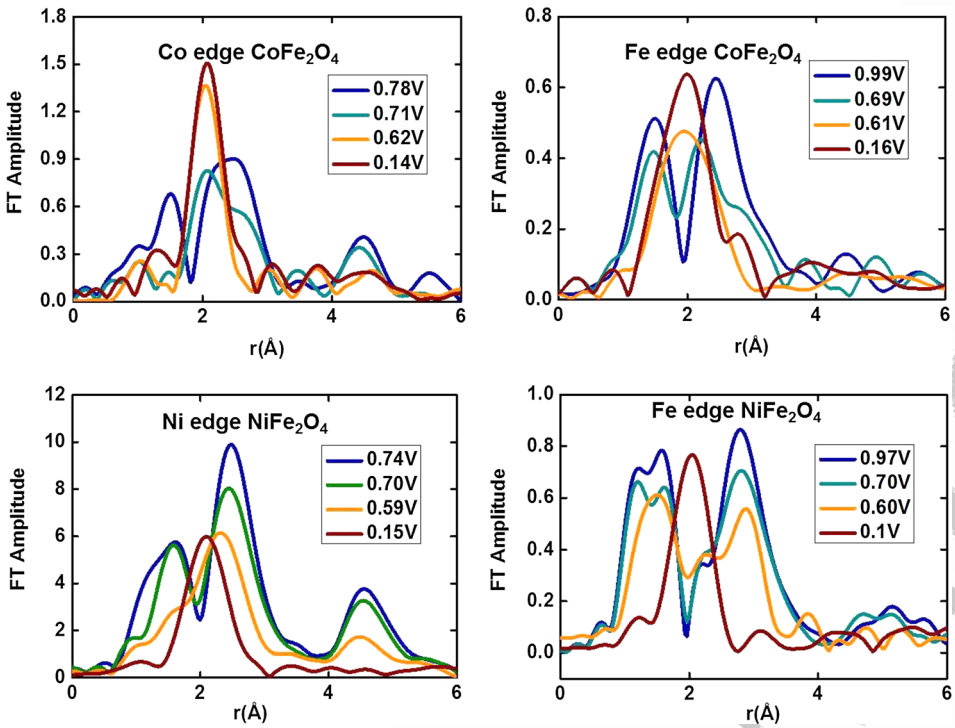

Figure 8. In situ FT spectra obtained for $CoFe_2O_4$ and $NiFe_2O_4$.

Table 3. EXAFS fitting results at the end of discharge. Coordination number (*N*), distance to the nearest neighbor (*r*), and Debye–Waller (*DW*) factors are fitted, and the results are tabulated. Amplitude reduction factors were obtained from reference materials and are fixed during the fitting

Edge	Sample	*CN* [N]	Interatomic distance (*r*) [Å]	*DW* factor [Å^2]
Fe	$CoFe_2O_4$	(Fe–Fe) 2.4	(Fe–Fe) 2.41(2)	(Fe–Fe) 0.005(2)
Fe	$NiFe_2O_4$	(Fe–Fe) 4.3	(Fe–Fe) 2.44(1)	(Fe–Fe) 0.013(1)
Co	$CoFe_2O_4$	(Co–Co) 4.9	(Co–Co) 2.41(2)	(Co–Co)0.009(2)
Ni	$NiFe_2O_4$	(Ni–Ni) 7.1	(Ni–Ni) 2.44(1)	(Ni–Ni) 0.020(2)

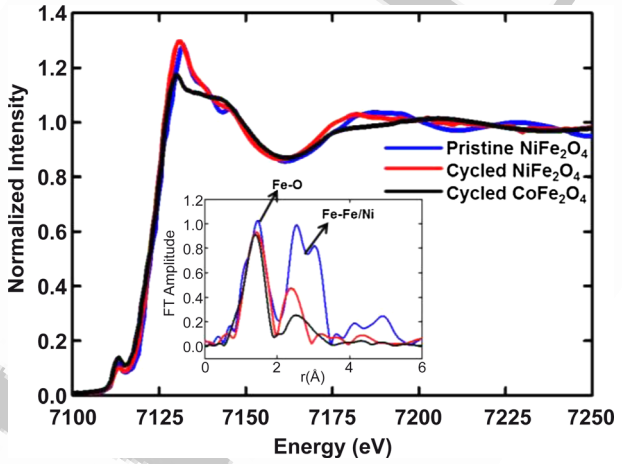

Figure 9. Fe K edge XANES region of cycled $CoFe_2O_4$ and $NiFe_2O_4$ materials. Inset: FT of the cycled materials. The XANES and FT of the cycled materials are compared with a pristine $NiFe_2O_4$ sample.

formed during the first discharging cycle are not completely transformed to their corresponding oxides. To get some quantitative information about the phase fraction, LCF fitting was applied to the cycled samples at the Co and Ni edges by using CoO and Co metal or NiO and Ni metal spectra as references, respectively. From the LCF fitting, about 60% of the Co and Ni remained in the metallic phase in the completely cycled, recharged sample. LCF fits of the Co and Ni edges are shown in Figure 11.

This phenomenon could be explained by the fact that the oxidation of Fe takes place at lower potentials than the oxidation of Co or Ni. Alternatively, the phenomenon could also be explained in terms of a kinetic effect, assuming a core–shell model of the metallic domains formed during the reduction process, with a Ni/Co core and an Fe shell. It is expected that, during the re-oxidation process, the Fe near the surface is preferentially oxidized compared to the Ni and Co, which are in the core. These metallic fractions may remain electrochemically inactive in the subsequent cycle, resulting in an overall reduction in the capacity.

3. Conclusions

Ternary transition-metal ferrites MFe_2O_4 (M = Co, Ni) synthesized through inverse co-precipitation were investigated as conversion-type model electrode systems in Li half-cells. In situ XAS studies performed at Fe, Co, and Ni K edges reveal that, during the conversion reaction, the ternary oxides transform into metal oxides, which are then subsequently reduced to the corresponding metallic states. From the EXAFS analysis, it was confirmed that the metallic phases formed are nano-structured. Finally, at the end of first cycle, it was found that Fe metallic domains, formed during the discharge, are completely re-oxidized. However, no such complete oxidation was observed for the Co and Ni metallic phases. The reason for the observed behavior can be attributed to the thermodynamically more favored formation of Fe_2O_3 in comparison with NiO or CoO. In addition, a kinetic limitation caused by the formation of a core–shell structure with a Ni/Co core and Fe shell could be suspected. The hindered re-oxidation of Co and Ni in the applied potential window could be the reason for the observed irreversible capacity loss in the first cycle for both materials. A higher reversible capacity and, hence, higher coulombic efficiency, especially in the initial cycle, would require a complete oxidation of Ni and Co at lower potentials. The cycling

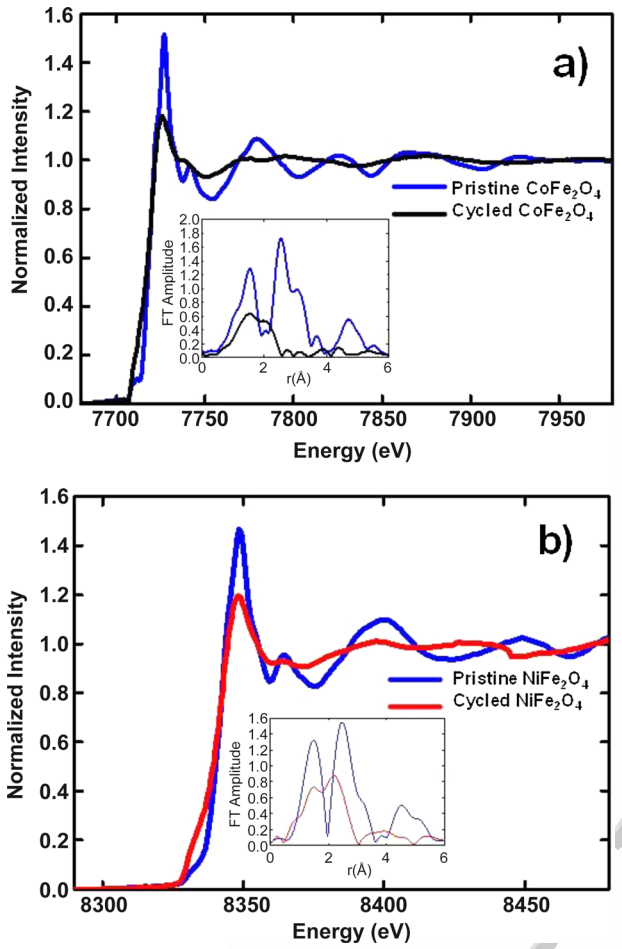

Figure 10. Co and Ni K edge XANES regions of cycled a) $CoFe_2O_4$ and b) $NiFe_2O_4$ materials. Insets: FT of the cycled material. XANES and FT of the cycled material are compared with those from pristine $CoFe_2O_4$ and $NiFe_2O_4$ samples.

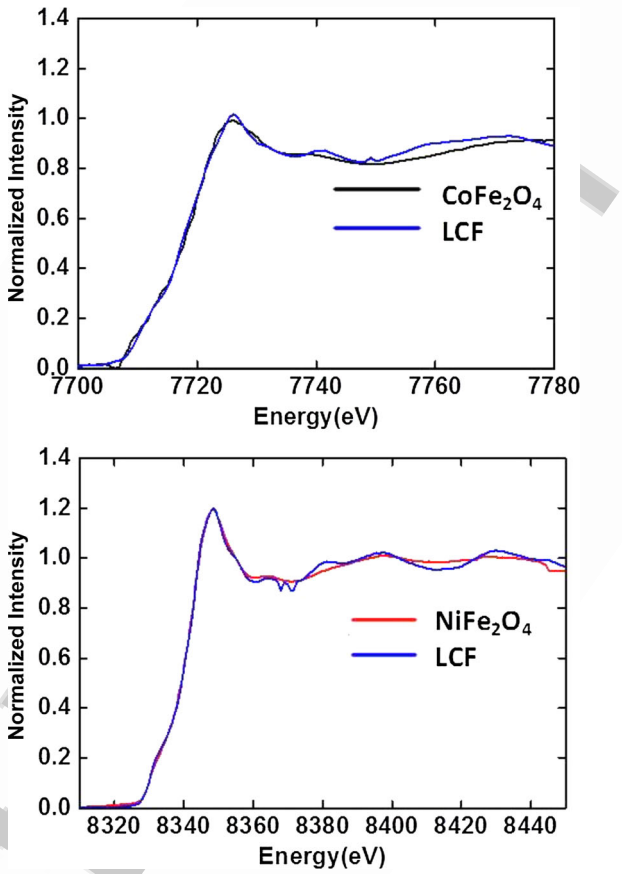

Figure 11. LCF fitting with CoO, Co metal, NiO, and Ni metal spectra as references for Co and Ni K edge XANES region of cycled a) $CoFe_2O_4$ and b) $NiFe_2O_4$ materials.

stability as well as coulombic efficiency could be improved by applying several strategies. These include the formation of nanocomposites with different carbon materials, thereby enhancing the electrical connectivity as well as forming a stable solid–electrolyte interphase. Another approach is electrode structuring by using methods such as electrospinning. In addition, combining a composite electrode with a suitable polymer binder and subjecting it to heat treatment could also bring out improvements in the electrochemical performance.[22–25]

Experimental Section

Synthesis of Spinel Ferrite Nanoparticles

Iron(II) acetate [$Fe(C_2H_3O_2)_2$], cobalt(II) acetate tetrahydrate [$Co(C_2H_3O_2)_2(H_2O)_4$], nickel(II) acetate tetrahydrate [$Ni(C_2H_3O_2)_2(H_2O)_4$], and sodium hydroxide [NaOH] were used for the synthesis and were purchased from Alfa Aesar, Germany. All reagents used for the synthesis were of analytical grade and used without further purification.

Syntheses of $NiFe_2O_4$ and $CoFe_2O_4$ were carried out by using a simple and environmental friendly inverse co-precipitation route.[26,27] Anhydrous iron acetate (0.4 M, 50 mL) and cobalt acetate tetrahydrate/nickel acetate tetrahydrate (0.2 M, 50 mL) were mixed in doubly distilled deionized water. The metal acetates were added to sodium hydroxide solution (1 M, 50 mL) drop wise with vigorous stirring. The addition of the reaction mixture to NaOH helps uniform mixing, which in turn helps us to obtain smaller and uniform particles. The solutions were heated and kept under stirring. The temperature was maintained at 80 °C for 1 h. The precipitates were centrifuged at 6000 rpm for 15 min and washed three times with deionized water to remove excess NaOH remaining in the precipitates. The obtained precipitates were then transferred into a drying oven and were dried at 85 °C overnight. The mixtures were then ground in a mortar, calcined at 800 °C at a heating rate of 400 °C h^{-1} for 4 h in air, and then cooled to room temperature without any explicit temperature control. The obtained substances were again ground into a very fine powder.

Electrode Preparation and Electrochemical Characterization

The electrodes of both $CoFe_2O_4$ and $NiFe_2O_4$ samples for XAS were prepared by mixing 60% (w/w) of the active material, 20% (w/w) super C 65 carbon (TIMCAL), and 20% (w/w) polyvinylidenefluoride (Solef PVdF 6020, Solvay) binder by grinding with acetone. About 15 mg of these mixtures for each material were pressed at a pressure of 8 tons on a copper mesh and dried at 110 °C for 1 h. CV investigations were performed for the obtained electrodes by using a two-electrode Swagelok cell. A lithium foil (Alfa Aesar) with 10 mm diameter and 0.75 mm thickness was used as the counter

and reference electrode. Two pieces of glass fiber (Whatmann-GF/D) separators with 12 mm diameter in size, wetted with 200 µL LP30 electrolyte [Merck, 1 M $LiPF_6$ in ethylenecarbonate (EC)/dimethylcarbonate (DMC) = 1:1], were used to separate the anode and counter electrode to eliminate a short circuit. The prepared cells were electrochemically cycled with a VMP3 multichannel potentiostat (Bio-Logic, France).

Crystal Structure and Morphology Characterization

The morphology investigations of initial powders were performed by using a Zeiss Supra 55 scanning electron microscope with primary electron energies of 5 and 15 keV and an in-lens detector. The particle size was calculated by using SmartTiffV2 software.

Powder XRD experiments for $CoFe_2O_4$ were performed for pristine samples at the powder diffraction beam line (MSPD) at ALBA, Barcelona, using synchrotron radiation with an energy of 30 keV (λ = 0.413486 Å) and a MYTHEN 1D position-sensitive detector. The powder diffraction data for $NiFe_2O_4$ was collected with a STOE STADI/P powder diffractometer equipped with a Dectris Mythen 1 K linear silicon strip detector and Ge (111) double crystal monochromator (Mo $K\alpha_1$ radiation; λ = 0.70926 Å). To perform these experiments, the samples were placed in 0.5 mm Ø quartz capillaries. Data analysis and structural refinement were performed with the Rietveld method using the Fullprof software package.[28]

In Situ and Ex Situ XAS Measurements: Setup and Cell Preparation

All in situ and most ex situ XAS measurements were carried out at the XAS beamline at ANKA, Karlsruhe. XAS spectra for $CoFe_2O_4$ and $NiFe_2O_4$ electrodes were recorded in transmission geometry with conventional step–scan mode at the Fe, Co, and Ni K edges during electrochemical cycling. Figure 12 shows the overview of the XAS

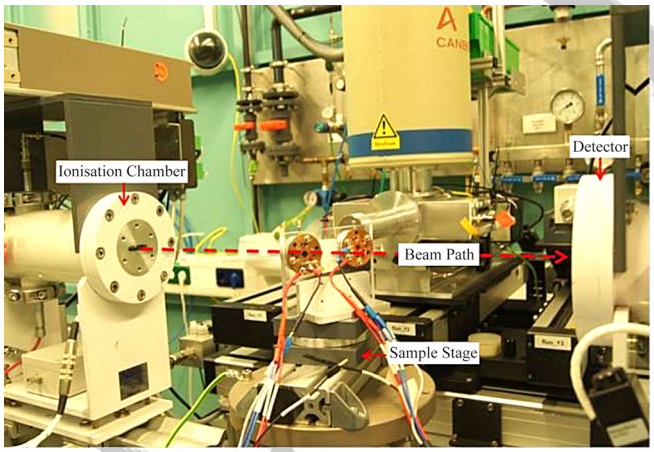

Figure 12. Overview of the XAS beamline at ANKA.

beamline at ANKA with the two-sample holder used. The ex situ XAS measurements on CoO and NiO reference materials were conducted at CLAESS, ALBA, Barcelona.

For ex situ measurements of the reference materials, about 10 g of the as-received powder materials was uniformly mixed with carboxy methyl cellulose in a mortar and pressed with 8 tons into a pellet. This dilution is performed so as to obtain the optimum edge jump for the XAS spectra. For in situ measurements, a modified version of the in situ cell reported in a previous work was used.[29] To get reasonably good transmission spectra, especially at the Fe edge, the glass window from one side of the in situ cell was replaced by a 500 µm-thin glassy carbon window. The in situ cells with both $CoFe_2O_4$ and $NiFe_2O_4$ samples were placed in the sample stage and separately aligned. The sample stage was moved automatically to shift between the samples, as shown in Figure 10. To measure the Fe, Co, and Ni edges in one run, the double-crystal fixed exit monochromator equipped with Si (111) crystals as well as the ionization chamber (IC Spec Ionisation Chamber, Oxford) were optimized for the Co edge. To detect the fluorescence signal, a five-element germanium detector (Ultra-LEGe Detector) was used. The positions of the electrochemical test cells and the energy ranges were all synchronized to facilitate the simultaneous in situ measurement of two samples at two different edges. To obtain reasonable time resolution, quick-EXAFS measurements were performed with a scan rate of 5 min for each spectrum. The spectra were processed by using the Demeter software package based on IFEFFIT and FEFF.[30] For each edge and for each sample, the fitting parameter involved a unique amplitude reduction factor S_0^2, which accounts for the relaxation of all the other electrons in the absorbing atom to the hole in the core level and an overall energy parameter (E_0). Moreover, each shell corresponding to an edge or sample was associated with a unique temperature factor or EXAFS Debye–Waller (*DW*) factors and interatomic distance parameters (*r*). All the EXAFS fittings were carried out in the *k* range of 2–12 $Å^{-1}$ and *r* range of 1–3 Å.

Acknowledgements

Financial support from DFG within the Research Priority Program SPP 1473, "Materials with new design for improved Li ion batteries-WeNDeLIB" under grant no EH183/16-2 is gratefully acknowledged. This work has benefitted from beam time allocation by the XAS beam line, ANKA, Karlsruhe, beam time by the materials science and powder diffraction beam line (MSPD), ALBA, and core-level absorption and emission spectroscopies (CLAESS), ALBA, Barcelona. Technical support from the beamline scientists, Dr. Francois Fauth and Dr. Marta Avila from MSPD and CLAESS, are gratefully acknowledged.

Keywords: conversion reaction · electrochemistry · negative electrodes · powder diffraction · X-ray absorption spectroscopy

[1] P. G. Bruce, B. Scrosati, J.-M. Tarascon, *Angew. Chem. Int. Ed.* **2008**, *47*, 2930 – 2946; *Angew. Chem.* **2008**, *120*, 2972 – 2989.
[2] P. Poizot, S. Laruelle, S. Grugeon, L. Dupont, J.-M. Tarascon, *Nature* **2000**, *407*, 496-499.
[3] S. Grugeon, S. Laruelle, R. Herrera-Urbina, L. Dupont, P. Poizot, J.-M. Tarascon, *J. Electrochem. Soc.* **2001**, *148*, A285.
[4] L. Ji, A. J. Medford, X. Zhang, *J. Mater. Chem.* **2009**, *19*, 5593.
[5] L. Ji, Z. Tan, T. R. Kuykendall, S. Aloni, S. Xun, E. Lin, V. Battaglia, Y. Zhang, *Phys. Chem. Chem. Phys.* **2011**, *13*, 7170 – 7177.
[6] B. Laik, P. Poizot, J.-M. Tarascon, *J. Electrochem. Soc.* **2002**, *149*, A251.
[7] D. Larcher, G. Sudant, J.-B. Leriche, Y. Chabre, J.-M. Tarascon, *J. Electrochem. Soc.* **2002**, *149*, A234.
[8] P. Poizot, S. Laruelle, S. Grugeon, J.-M. Tarascon, *J. Electrochem. Soc.* **2002**, *149*, A1212.
[9] N. Pereira, L. C. Klein, G. G. Amatucci, *J. Electrochem. Soc.* **2002**, *149*, A262.

[10] N. Pereira, L. Dupont, J. M. Tarascon, L. C. Klein, G. G. Amatucci, *J. Electrochem. Soc.* **2003**, *150*, A1273.
[11] R. D. Apostolova, E. M. Shembel', I. Talyosef, J. Grinblat, B. Markovsky, D. Aurbach, *Russ. J. Electrochem.* **2009**, *45*, 311 – 319.
[12] a. Débart, L. Dupont, R. Patrice, J. M. Tarascon, *Solid State Sci.* **2006**, *8*, 640 – 651.
[13] Y. Kim, J. B. Goodenough, *J. Phys. Chem. C* **2008**, *112*, 15060 – 15064.
[14] L. Ji, Z. Lin, M. Alcoutlabi, X. Zhang, *Energy Environ. Sci.* **2011**, *4*, 2682.
[15] Q. Su, D. Xie, J. Zhang, G. Du, B. Xu, *ACS Nano* **2013**, *7*, 9115 – 9121.
[16] M. C. Menard, K. J. Takeuchi, A. C. Marschilok, E. S. Takeuchi, *Phys. Chem. Chem. Phys.* **2013**, *15*, 18539 – 18548.
[17] Z. Quan, E. Ni, Y. Ogasawara, N. Sonoyama, *Solid State Ionics* **2014**, *262*, 128 – 132.
[18] C. Yuan, H. Bin Wu, Y. Xie, X. W. Lou, *Angew. Chem. Int. Ed.* **2014**, *53*, 1488 – 1504.
[19] P. Lavela, J. L. Tirado, *J. Power Sources* **2007**, *172*, 379 – 387.
[20] R. Alcántara, M. Jaraba, P. Lavela, J. L. Tirado, J. C. Jumas, J. Olivier-Fourcade, *Electrochem. commun.* **2003**, *5*, 16 – 21.
[21] M. H. Nilsen, C. Nordhei, A. L. Ramstad, D. G. Nicholson, M. Poliakoff, A. Cabanas, *J. Phys. Chem. C* **2007**, *111*, 6252 – 6262.
[22] L. Wu, Q. Xiao, Z. Li, G. Lei, P. Zhang, L. Wang, *Solid State Ionics* **2012**, *215*, 24 – 28.
[23] S. Peng, L. Li, M. Srinivasan, *J. Energy Chem.* **2014**, *23*, 301 – 307.
[24] Y.-H. Jin, S.-D. Seo, H.-W. Shim, K.-S. Park, D.-W. Kim, *Nanotechnology* **2012**, *23*, 125402.
[25] J. Cabana, L. Monconduit, D. Larcher, M. R. Palacín, *Adv. Mater.* **2010**, *22*, E170 – 92.
[26] X. Yang, X. Wang, Z. Zhang, *J. Cryst. Growth* **2005**, *277*, 467 – 470.
[27] P. Reddy, Y. Raja, M. Ashok, *Adv. Mater. Res.* **2014**, *895*, 287 – 290.
[28] T. Roisnel, J. Rodriguez-Carvajal, *Mater. Sci. Forum* **2001**, *378*, 118 – 123.
[29] M. Herklotz, F. Scheiba, M. Hinterstein, K. Nikolowski, M. Knapp, A. C. Dippel, L. Giebeler, J. Eckert, H. Ehrenberg, *J. Appl. Crystallogr.* **2013**, *46*, 1117 – 1127.
[30] B. Ravel, M. Newville, *J. Synchrotron Radiat.* **2005**, *12*, 537 – 541.

Received: May 6, 2015
Published online on ■■ ▮▮, 2015

ARTICLES

G. Balachandran, D. Dixon, N. Bramnik, A. Bhaskar, M. Yavuz, L. Pfaffmann, F. Scheiba, S. Mangold, H. Ehrenberg*

■■ – ■■

Elucidation of the Electrochemical Reaction Mechanism in MFe_2O_4 (M = Ni, Co) Conversion-Type Negative Electrode Systems by using In Situ X-ray Absorption Spectroscopy

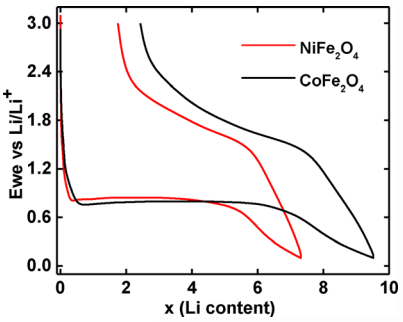

X-ray vision: The mechanism of Li insertion–deinsertion in model conversion-type anode systems of MFe_2O_4 (M = Ni, Co) is investigated through an in situ X-ray absorption spectroscopic investigation. The main focus is to understand the reason behind irreversible capacity losses in these materials.

#InSitu #XAS study into #electrochemical mechanism of conversion #anode systems @KITKarlsruhe SPACE RESERVED FOR IMAGE AND LINK

Share your work on social media! *ChemElectroChem* has added Twitter as a means to promote your article. Twitter is an online microblogging service that enables its users to send and read text-based messages of up to 140 characters, known as "tweets". Please check the pre-written tweet in the galley proofs for accuracy. Should you or your institute have a Twitter account, please let us know the appropriate username (i.e., @accountname), and we will do our best to include this information in the tweet. This tweet will be posted to the journal's Twitter account @ChemElectroChem (follow us!) upon online publication of your article, and we recommended you to repost ("retweet") it to alert other researchers about your publication.